



Internal flow effect on particle transport in an evaporating colloidal sessile droplet

Mebrouk AIT SAADA^{1a}, Salah CHIKH^{1b}, Lounès TADRIST^{2c}

¹USTHB, Faculty of Mechanical and Process Engineering, LTPMP, Alger 16111, Algeria

²Aix-Marseille Université, CNRS, Laboratoire IUSTI, UMR 7343, Marseille 13453, France

^a*m_aitsaada@yahoo.fr*, ^b*salahchikh@yahoo.fr*, ^c*lounes.tadrist@univ-amu.fr*

Abstract: The effect of internal flow on the transport of particles in an evaporating water sessile droplet is investigated numerically. Flow and heat transfer as well as the transport of colloids in the droplet, heat conduction in the substrate and surrounding air, and vapor diffusion in the gas phase are taken in account in the developed numerical model. The finite volume method is adopted to work out the problem and to predict how the colloids are distributed inside the droplet. The results show that the internal flow in the drop affects the distribution of the concentration of the solid particles during the evaporation. The outgoing radial flow tends to transport the particles to the edge of the drop towards the contact line, while the flow induced by thermo-capillarity, with its cellular pattern, tends to carry the particles from the edge towards the core of the droplet.

Keywords: sessile droplet evaporation, colloidal suspension, thermo-capillarity, particles deposition

1. Introduction

The evaporation of drops of colloidal suspension is a phenomenon that may be encountered in many technological applications such as the biological organization of deposits of protein particles or DNA and the manufacture of micro and nanowires or nanocrystals. The deposition patterns left after evaporation have ring-like structures or more complex shapes. Controlling the distribution of solute during drying is vital in many industrial and scientific processes. For example, paint manufacturers use a variety of additives to ensure that the pigment is evenly dispersed and remains so during drying. Segregation effects are undesirable in this case. However, as in the production of nanowires, ring effect can be a boon. Understanding the deposit formation process should be of interest to those attempting to circumvent or harness the ring deposition phenomenon.

A literature survey shows that a great attention is paid to the drop stain left after evaporation. Deegan et al. [1-3] explained the formation of deposits by a strong radial flow carrying particles towards the pinned contact line. Onoda and Somasundaran [4] evidenced the effect of the chemical or physical heterogeneity of the substrate on the final drop stain. Maenosono et al. [5] observed that the ring of nanoparticles is formed in two steps. During a first step, the contact line remains pinned and the particles accumulate at the periphery of the drop; then in a second step, the contact line is receding. Shmulyovich et al. [6] studied the formation of multiple rings for drying cases of water droplets of 1 to 70 μl , containing latex particles of 0.88 to 3.15 μm in diameter. The formation of the solid ring occurs through a succession of hooked contact line. The flow direction within the evaporating sessile droplet can also influencing the deposition traces. Hu and Larson [7] observed that the induced Marangoni effect had a preferential deposition at the center of the drop rather than at the periphery. Bhardwaj et al. [8] studied numerically the formation of particle deposits during the drying of drops of nanoliter size. The results of their numerical model showed that the direction of the Marangoni flow inside the drop is controlled by the ratio of thermal conductivity of the PDMS substrate over that of isopropanol liquid. Fischer [9] used the lubrication theory to study numerically the advection of particles and presented their transient distribution within the drop.

The analysis of the literature review shows that despite the many technological applications of colloidal sessile droplet evaporation and the importance for understanding this physical phenomenon, there are a limited number of works on particle deposition. The present work is a numerical study of the effect of internal flow on the transport of diluted particles in a sessile drop of water during evaporation. The flow inside the drop may be

induced by the large evaporation rate near the contact line, by the thermal buoyancy in the liquid phase if large temperature gradient is present and/or by the thermo-capillary effect due to the variation of the surface tension along the drop surface. The objective is to show how the type of internal flow governs the drop stain after drying.

2. Problem statement and mathematical formulation

A 10 mm³ colloidal suspension droplet is resting on a horizontal substrate of radius R_∞ and thickness e_s . The extent of the substrate is considered as being very large ($R_\infty \approx 200 R$, R being the droplet radius). A very thin layer of Aluminum that imposes an initial contact angle θ_0 of 78° covers the upper face of the substrate [10]. The small size of the droplet makes that the surface tension force is prevailing over the gravity force and we may assume that the droplet has a spherical shape. The surrounding air is at a temperature T_∞ of 25°C and a relative humidity H_a of 40% far away from the droplet. The present study considers the case where the lower face of the substrate is at a temperature T_w of 25°C (unheated case) and the evaporation occurs in a stick mode i.e. the contact line is pinned and the contact radius remains constant while the contact angle varies over time [10]. Figure 1 illustrates the computational domain and the boundary conditions.

The domain is divided into three zones. Cylindrical coordinates are used in zone I corresponding to the solid substrate, toroidal coordinates in zone II of hemispherical shape that encompasses the liquid droplet and part of the surrounding air and spherical coordinates in zone III that includes the remaining domain. The toroidal coordinates employed in zone II allow locating accurately the liquid-gas mobile interface with a single value of the coordinate β .

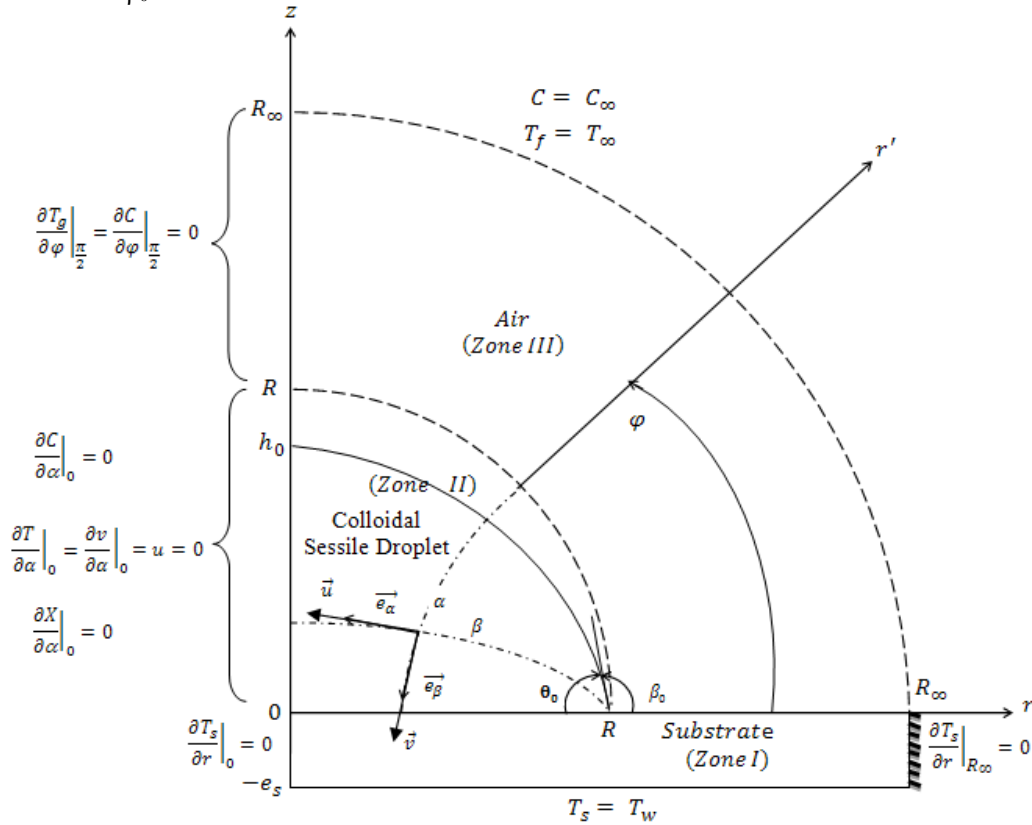


Figure 1: Computational domain and the boundary conditions. A colloidal suspension droplet is resting on a horizontal substrate of radius R_∞ and thickness e_s .

The mathematical formulation based on conservation equations i.e. mass, momentum, energy and particles concentration is written in a general form [11]. The flow inside the droplet is governed by the Navier-Stokes equations, it is induced by the strong evaporation rate at the contact line, the thermo-capillarity and the thermal buoyancy. The Boussinesq approximation is made to model thermal buoyancy and thermo-capillary effect is included through the variation of surface tension with temperature at the liquid-gas interface. Convective heat and mass transfers in liquid phase are obtained by resolving the energy and colloids concentration equations. In the surrounding air, heat and vapor transport are modeled by diffusion equations. Heat conduction equation is used in the solid phase. All the transport phenomena induced by the phase change

are assumed to occur in a quasi-steady state because of the very slow motion of the droplet surface during evaporation.

The governing equations are put in dimensionless form based on the reference length R which is the base radius of the droplet and the reference velocity $\frac{d\sigma}{dT} \frac{\Delta T}{\mu_l}$ which is the capillary velocity. The dimensionless variables of position, velocity and pressure are indicated by a star in superscript. The dimensionless variables of temperature, vapor concentration and colloid concentration are:

$$T^* = \frac{T - T_\infty}{\Delta T}, \quad C^* = \frac{c - c_\infty}{\Delta c}, \quad X^* = \frac{X}{\frac{1}{V_d} \int X dV_d}$$

where $\Delta T = D(1 - H_a) C_v(T_\infty) h_{lg}/k_l$, $\Delta c = C_w - C_\infty$ with $C_w = C_v(T_w)$ and $C_\infty = H_a C_v(T_w)$

Then the dimensionless governing equations are cast in the form:

i) in liquid phase

$$\vec{\nabla} \cdot \vec{W} = 0 \quad (1)$$

$$(\vec{W} \cdot \vec{\nabla}) \vec{W} = -\vec{\nabla} P + \frac{Pr}{Ma} \Delta \vec{W} - \frac{Ra Pr}{Ma^2} T_\ell^* \vec{I} \quad (2)$$

$$(\vec{W} \cdot \vec{\nabla}) T_\ell^* = \frac{1}{Ma} \Delta T_\ell^* \quad (3)$$

$$(\vec{W} \cdot \vec{\nabla}) X^* = \frac{1}{Ma Le_l} \Delta X^* \quad (4)$$

\vec{W} is the velocity vector and $\vec{I} = -\vec{e}_z$ is the unit vector.

ii) in gas phase

$$\Delta T_g^* = 0 \quad (5)$$

$$\Delta C^* = 0 \quad (6)$$

iii) in solid phase

$$\Delta T_s^* = 0 \quad (7)$$

The associated dimensionless boundary conditions are indicated in fig.1 and the dimensionless conditions at liquid-gas interface are written as [12]:

a) Mass conservation

$$v^* = -\sqrt{1 - (\sin\theta r^*)^2} V_{IZ}^* - \frac{R_{\alpha T} (\Delta C / \rho)}{Le_g Ma} J^* \quad (8a)$$

with V_{IZ}^* being the velocity of the moving interface,

$$V_{IZ}^* = -8 \left(\frac{\cos(\theta/2)}{\sin\theta} \right)^2 \left(1 - \frac{1}{h^* \tan\theta + 1} \right) \left(\frac{R_{\alpha T} (\Delta C / \rho)}{Le_g Ma} \right) \frac{\dot{M}^*}{(1 + h_0^{*2})} \text{ and } h_0^* = \tan(\theta/2)$$

V_{IZ}^* is obtained basing on the drop geometry given by the shape of a spherical cap. We note that h_0^* is the height of the drop apex and $R_{\alpha T}$ is a thermal diffusivity ratio (gas/liquid).

b) Mechanical Equilibrium,

$$\frac{\partial u^*}{h^* \partial \beta} + \frac{\partial v^*}{h^* \partial \alpha} + \sin\beta u^* + \sinh\alpha v^* = \frac{\partial T_\ell^*}{h^* \partial \alpha} \quad (8b)$$

The left-term of equation (8b) expresses the viscous effect due to the shear stress in liquid and the right-term is the thermo-capillary effect involving the temperature gradient along the interface.

c) Thermal Equilibrium,

$$T_\ell^* = T_g^* \quad (1c)$$

d) Heat Balance,

$$\left(\frac{\Delta C}{\rho} \right) \frac{R_{\alpha T} J_a}{Le_g} J^* - \frac{\partial T_\ell^*}{h \partial \beta} + RK_g \frac{\partial T_g^*}{h \partial \beta} = 0 \quad (1d)$$

e) Saturation Concentration,

$$C^* = \frac{C_V(T) - C_\infty}{\Delta C} \quad (1e)$$

where $C_V(T)$ is computed using a polynomial relationship of fourth power.

$$C_V(T) = \sum_{i=0}^4 a_i T^i \quad (1f)$$

The coefficients a_i are selected to fit the experimental data of Raznjevic [13].

f) Colloids Concentration with a zero mass flux,

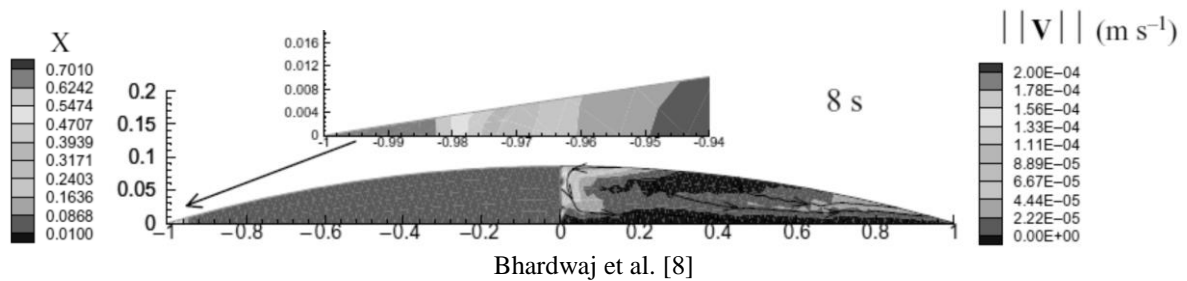
$$v^* X^* - \frac{1}{Ma Le_l} \frac{\partial X^*}{\partial \beta} = 0 \quad (1g)$$

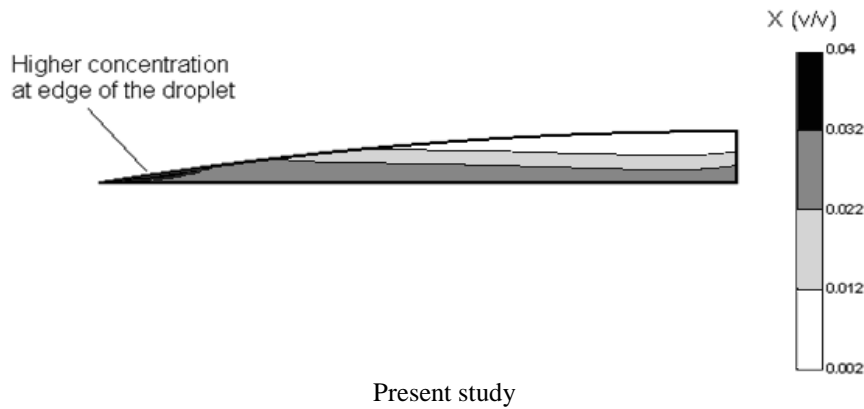
Several dimensionless numbers appear in the governing equations and the conditions at liquid-gas interface. These are the controlling parameters of the study, namely the Prandtl number $Pr = \left(\frac{v}{\alpha_T}\right)_l$, the Marangoni number $Ma = \left(\frac{d\sigma}{dT} \Delta T R\right) / (\mu \alpha_T)_l$, the Rayleigh number $Ra = \frac{g(\beta_T)_l \Delta T R^3}{(v \alpha_T)_l}$, the Lewis number with respect to vapor diffusion in air $Le_g = \frac{\alpha_T g}{D}$, the Lewis number with respect to colloids diffusion in the droplet $Le_l = \frac{\alpha_T l}{D_{pl}}$, the thermal conductivity ratio RK (gas/liquid and solid/liquid), the thermal diffusivity ratio R_{α_T} (gas/liquid), the Jacob number $Ja = \frac{h_{lg}}{(c_p)_l \Delta T}$ and the ratio of the concentration difference over the density of water $\left(\frac{\Delta C}{\rho_l}\right)$.

3. Numerical procedure

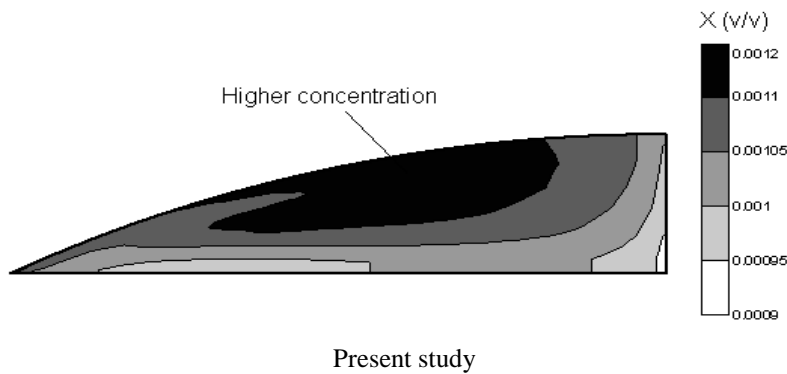
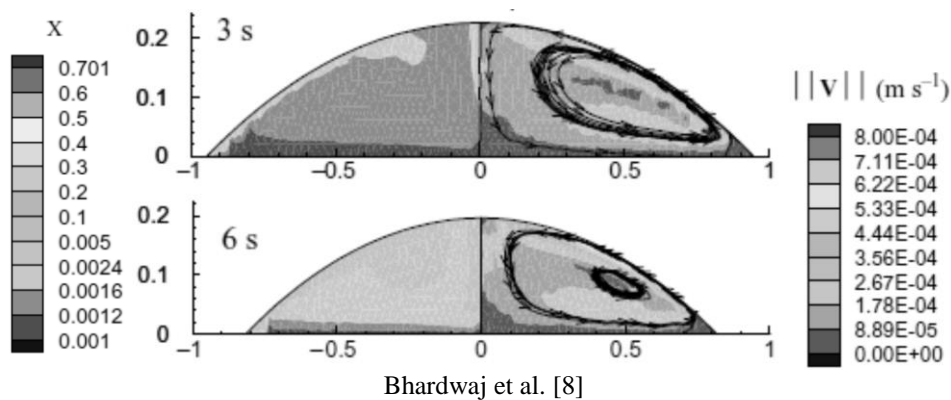
The governing equations (1-8) with the corresponding boundary conditions and interfacial conditions are solved by means of the finite volume method [14]. Staggered grids are utilized in the drop with a very fine cell size, of the order of $10^{-4}R$, around the contact line in the three phases. The velocity-pressure coupling is handled using the SIMPLE algorithm (Semi Implicit Method for Pressure Linked Equations). The PLDS (Power Law Differencing Scheme) is adopted to discretize convection and diffusion terms. The solution method of the system of algebraic equations is based on a combination of Thomas Algorithm and the Gauss-Seidel point iterative method. Several convergence criteria of the iterative process are set. The solution is reached once the maximum relative error on each dependent variable (u^* , v^* , T^* , C^* , X^*) is less than 0.1%, the maximum residue of each conservation equation is less than 10^{-5} and the maximum allowable residue of continuity equation is less than 10^{-10} .

The implemented computer program is validated by comparing our results with results of Bhardwaj et al. [8] who studied numerically the formation of particles deposit after drying of sessile drops. Figure 2 displays the velocity and particle concentration fields inside the drop. A fairly good agreement exists between our results and those of Bhardwaj et al. [8]. In the case of internal flow induced by the strong evaporation near the contact line, the largest concentration of particles is noted at the edge of the drop as illustrated in Fig. 2 (a). When the flow is driven by thermo-capillary effect, the maximum particles concentration is rather located in the core of the drop (Fig.2b). Thus, it is confirmed that our numerical simulations reproduce reliably the particles distribution inside the sessile drop under the effect of the internal flow during the evaporation.





a) Radial flow due to strong evaporation at contact line. Colloidal suspension droplet of water with initial particle concentration of 1% on a glass substrate.



b) Thermo-capillary flow in colloidal suspension droplet of isopropanol with an initial particle concentration of 1.0% on a polydimethylsiloxane (PDMS) substrate.

Figure 2 : Comparison with results of Bhardwaj et al. [8]
 (a) $V_0 = 3.7 \text{ nL}$, $\theta_0 = 22^\circ$, (b) $V_0 = 38 \text{ nL}$, $\theta_0 = 32^\circ$.

4. Results and discussion

The numerical results are presented for a case of a colloidal water droplet of 10 mm^3 initial volume resting on a substrate of aluminum (unheated case). The first part of results considers the evaporation of a pure water droplet without thermo-capillary effect and then including it in order to show its influence on the dynamic, thermal and solutal aspects. The second part is devoted to study the effect of flow on the transport of colloids within the droplet.

Figure 3 exhibits the velocity field and the streamlines inside the drop for different contact angles. For the case without thermo-capillary effect, a cellular flow with a clockwise motion is displayed at high values of the contact angle ($\theta \geq 50^\circ$). Very quickly, this flow, influenced by the thermal buoyancy, tends to dissipate as the evaporation process evolves ($\theta < 50^\circ$), giving way to an outward radial flow due to the privileged evaporation

near the contact line. When including the thermo-capillary effect, the thermal buoyancy and evaporation effects become very weak and a counter-clockwise cellular flow sets up. The liquid moves from the contact line toward the drop apex along the liquid-gas interface with much higher velocity as compared to the case without thermo-capillary effect, but decreasing over time. This flow is imposed by the surface tension gradient along the drop surface, which is, itself, due to temperature gradient. This cellular flow remains throughout the evaporation, except at the end where it becomes outward radial flow. The liquid velocity is higher at the drop surface than near the solid-liquid interface because of the adherence at the solid wall.

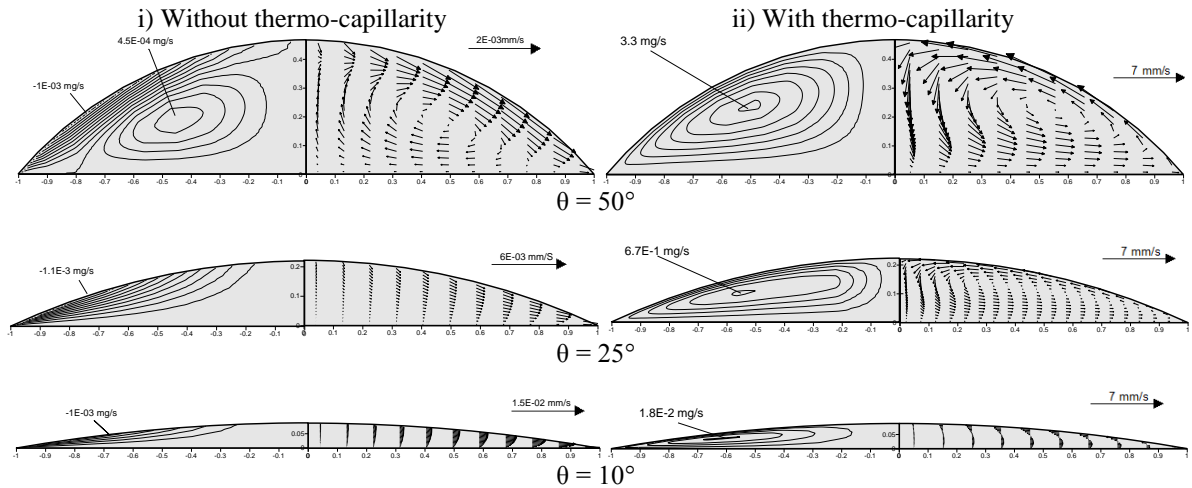
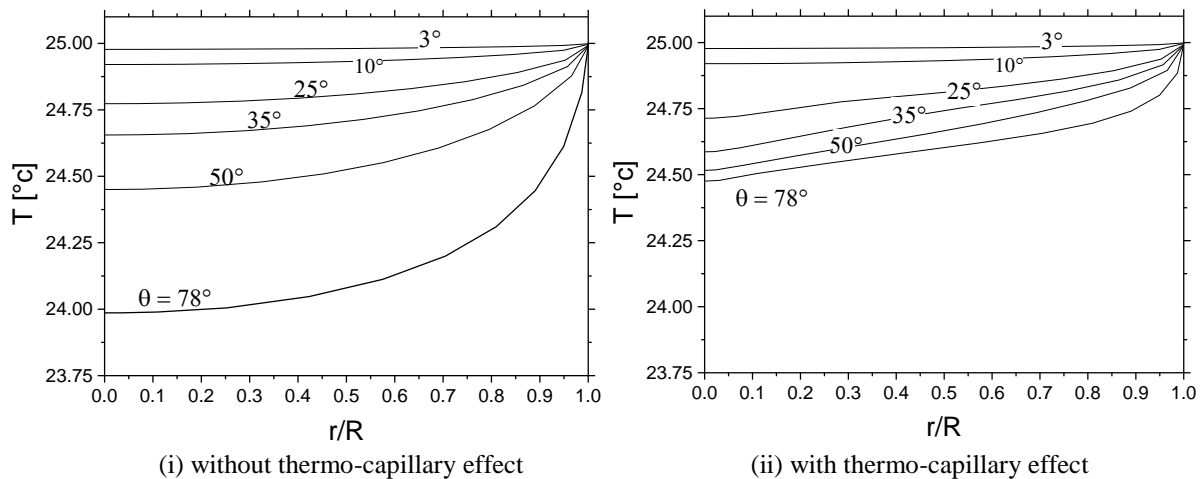


Figure 3: Streamlines (left) and velocity field (right) for different contact angles for a pure water droplet. Two cases are considered: i) without thermo-capillary effect, ii) with thermo-capillary effect.

Figure 4a illustrates the temperature profile along the drop surface. It is evidenced that the temperature decreases from its maximum value at the contact line to its minimum value at the drop apex regardless of the contact angle. Furthermore, the temperature at the drop surface increases during the evaporation process, that is the cooling effect is important at the beginning and then diminishes over time. This temperature profile allows assessment of the importance of the temperature gradient along the liquid-gas interface and consequently its impact on the importance of the thermo-capillary effect. It can be deduced that the thermo-capillary effect decreases with time and vanishes at small contact angles. Further to evaporation, the drop surface cools down, but the thermo-capillary flow supplies heat from the substrate to the drop surface and reduces the cooling effect. Figure 4b plots the flux of evaporation rate versus the radial position along the drop surface. The local heat exchange in the liquid phase strongly influences the flux of evaporation. The local mass loss at the liquid-gas interface augments substantially near the contact line and increases over time in this zone when the contact angle decreases. However, it remains almost constant outside the vicinity of the contact line and it undergoes a decrease over time. This evaporation rate per unit area is one of the factors controlling the flow within the drop, especially near the contact line. Indeed, the flow velocity is high because of the relatively large mass transfer in this zone. However, it is noted that the influence of thermo-capillarity on the mass loss by evaporation is low, as shown by comparing the results presented in Fig.4b (i) and Fig.4b (ii).



a) Temperature profiles

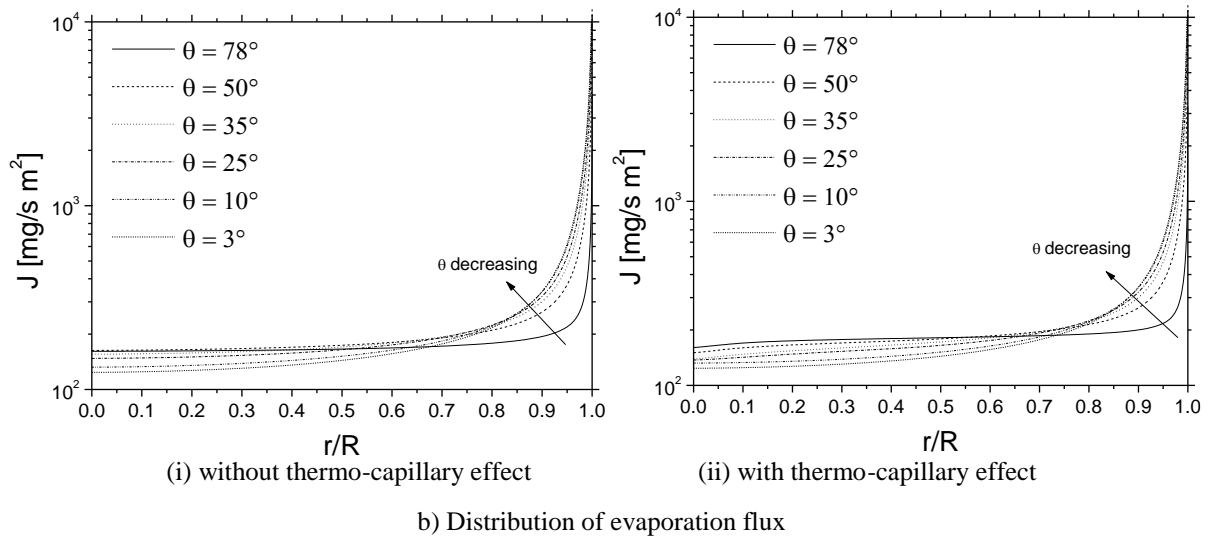


Figure 4 : Temperature profile and evaporation flux along the drop surface for different values of the contact angle. Two cases are considered: i) without thermo-capillary effect, ii) with thermo-capillary effect.

Figure 5 presents the evolution of the global evaporation rate versus the contact angle including or not the thermo-capillary effect. The evaporation rate \dot{M} decreases over time as the contact angle decreases. The local temperature at the drop surface increases during evaporation and thus induces an increase in the concentration of vapor saturation. However, the reduction of the drop surface area remains greater and yields a decrease of the evaporation rate. This latter is slightly larger for the case with thermo-capillary effect at large contact angles. The difference decreases gradually until the same evaporation rate is obtained for the small contact angles, meaning that the thermo-capillary convective effects become negligible.

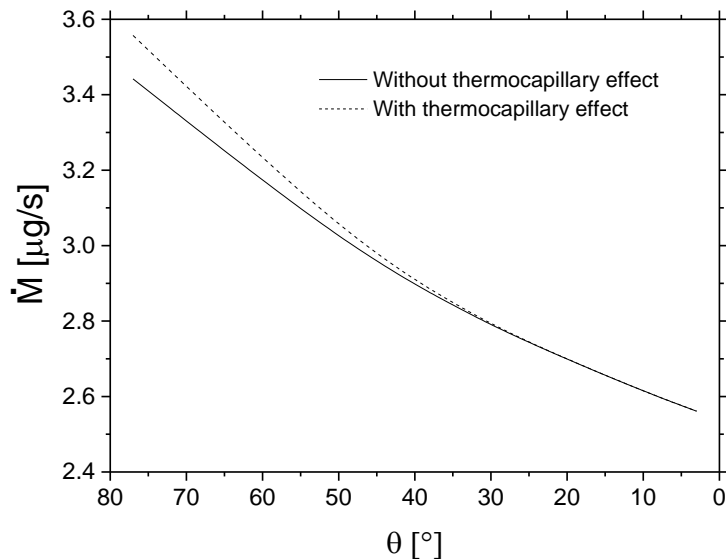


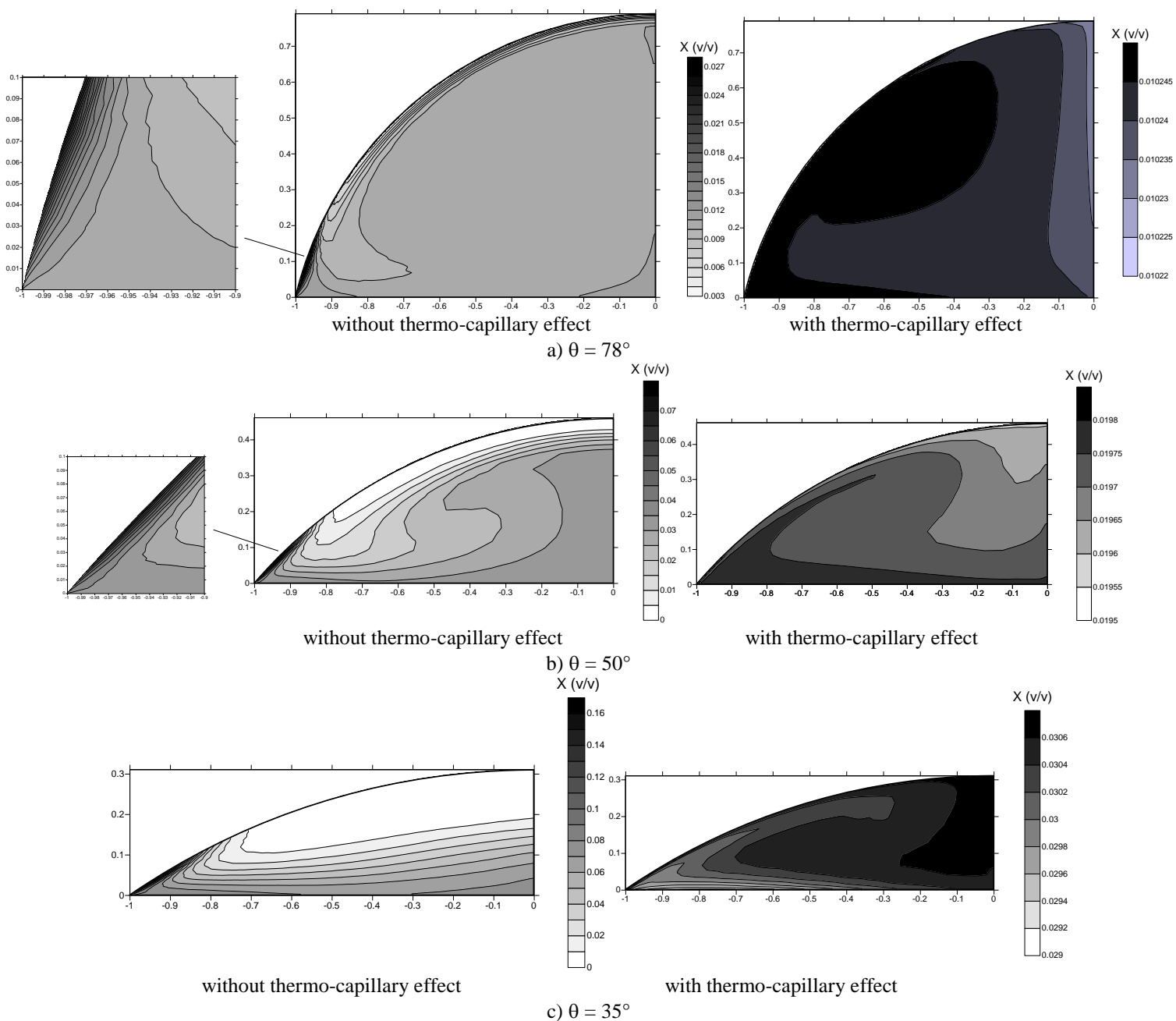
Figure 5: Evolution of global evaporation rate versus the contact angle for both cases with and without thermo-capillarity.

The results presented next relate to the analysis of the impact of the internal flow (with or without thermo-capillary effect) on the distribution of particle concentration in a sessile drop of colloidal water during the evaporation. The solid particles, diluted in liquid water with an initial concentration of 1% (v/v), are made of polystyrene with a diameter of 100 nm. The initial volume of the drop is 10 mm³ identical to that of the evaporation of a pure water drop and the initial contact angle is 78°. The diffusion coefficient of polystyrene particles in liquid water is 4x10⁻¹² m²/s as given in [8]. This value is relatively low implying colloids transport strongly influenced by the internal flow.

Figure 6 illustrates the results of the concentration field X for different contact angles during evaporation. The values of the contact angle are selected to browse the whole process of evaporation from the beginning to the end. In order to depict the two effects of internal flow due to the privileged evaporation rate near the contact line and the thermo-capillary flow, results are presented for the two cases.

For the various stages of evaporation, the radial flow, i.e. without the thermo-capillary effect, induces the particle distribution with a high concentration toward the contact line. This confirms the drop stain after drying that shows the particle deposit stuck up in the edge of the drop as long as the contact line remains pinned as reported experimentally by Deegan et al. [1] and numerically by Bhardwaj et al. [8]. This result also corresponds to the theory of Deegan et al. [2] for evaporating sessile droplets with small contact angles, a viscous internal flow and without evaporative cooling.

If we now consider the thermo-capillary flow, which is a counter clockwise cellular pattern as previously shown in Fig.2, then the flow, with its high velocity at the liquid-gas interface, conveys the particles from the edge to the core of the drop. This explains the high particle concentration near the drop surface. Nevertheless, this mechanism of particle transport due to the effect of thermo-capillarity vanishes towards the end of the evaporation, leaving the effect of the radial flow prevail over the remaining short time. Consequently, it can be concluded that the solid particles, after drying, would deposit on the substrate, particularly, in the core zone of the drop as Bhardwaj et al. [8] have already showed it numerically. It must be also noted that the theory of Deegan et al. [2] remains applicable towards the end of evaporation where the thermo-capillary effect is negligible. Before this, the internal transport of particles is influenced by a cellular flow due to the evaporative cooling of the droplet.



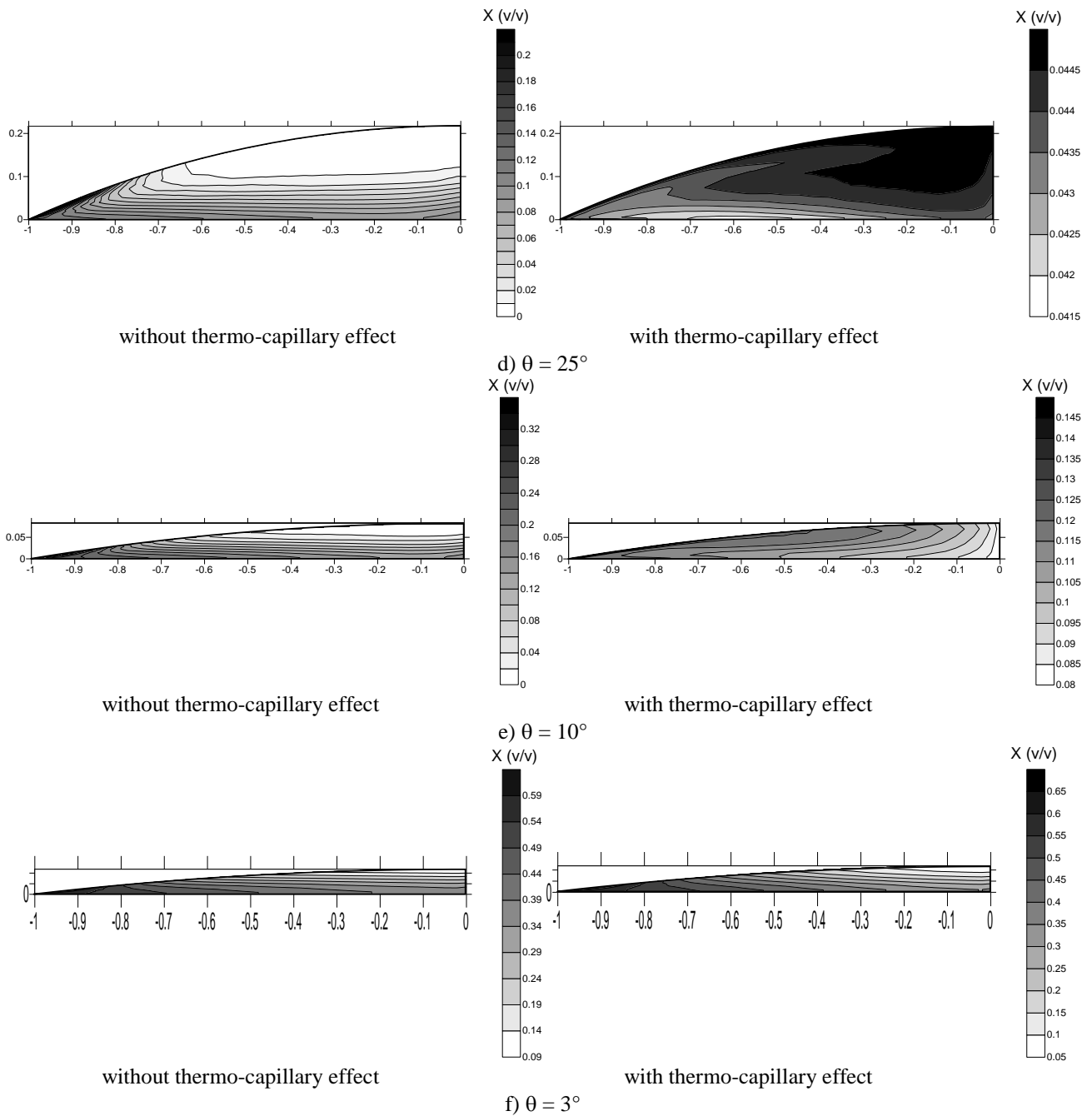


Figure 6: Colloids concentration field in the drop for different contact angles. The values of the contact angle are selected to browse the whole process of evaporation from the beginning to the end. Results are presented for the two effects of internal flow due to the privileged evaporation rate near the contact line and the thermo-capillary flow.

5. Conclusion

In the present work, we investigated numerically the effect of internal flow on the transport of particles diluted in a sessile drop of water. The obtained results showed that the flow inside the drop can be induced by the high evaporation rate close to the contact line or by the thermo-capillarity due to the cooling effect produced by the liquid-vapor phase change. The evaporation rate is weakly influenced by the convective thermo-capillary effect inside the drop; this is much more exhibited at large contact angles. The flow inside the sessile drop of colloidal suspension imposes the distribution of solid particle concentration during evaporation. The outgoing radial flow tends to transport the particles to the edge of the drop, which yields the formation of a solid annular deposit after drying (coffee stain effect). The thermo-capillary induced cellular flow tends to carry the particles from the edge towards the drop core, which yields the formation of a particles deposit around the center of the

drop. As perspective, we consider the improvement of the present numerical model for predicting the particle deposition patterns and their geometric characteristics.

Nomenclature

C	Concentration	[kg/m ³]	R	Drop contact radius	[m]
C_v	Saturated vapor concentration	[kg/m ³]	r, z	Cylindrical coordinates	[m]
D	Vapor diffusion coefficient in air	[m ² /s]	r', φ	Spherical coordinates	[m]
D_{pl}	Particle diffusion coefficient in liquid	[m ² /s]	T	Temperature	[°C]
e_s	Thickness of solid substrate	[m]	u, v	velocity component	[m/s]
h_0	Height of the drop apex	[m]	V_d	Drop volume	[m ³]
H_a	Relative humidity of air		X	Particle concentration	[V/V]
h_{lg}	Latent heat of vaporization	[J/kg]	Greek Symbols		
$h_{\alpha, \beta, \phi}$	Metric coefficients ($h = h_\alpha = h_\beta$)	[m]	α, β, φ	Toroidal coordinates	[rd]
J	Evaporation flux	[kg/m ² s]	θ	Contact angle	[rd]
Ja	Jacob number	[-]	α_T	Thermal diffusivity of liquid	[m ² /s]
k	Thermal conductivity	[W/m K]	μ	Dynamic viscosity of liquid	[kg/m s]
Le_g	Lewis number (in gas)	[-]	ρ	Density of liquid	[kg/m ³]
Le_l	Lewis number (in liquid)	[-]	σ	Surface tension	[N/m]
Ma	Marangoni number	[-]	Subscripts		
\dot{M}	Evaporation rate	[kg/s]	g, l, s	Gas, liquid, solid	
P	Pressure	[Pa]	w	Upper surface of the substrate	
Pr	Prandtl number	[-]	∞	At infinity	
Ra	Rayleigh number	[-]	Superscripts		
R_k	Thermal conductivity ratio	[-]	*	Dimensionless variable (u^*, v^*, P^*, T^*, X^*)	

References

- [1] Deegan R. D., Bakajin O., Dupont T. F., Huber G., Nagel S. R. and Witten T. A., 1997 Capillary flow as the cause of ring stains from dried liquid drops, *Nature* 389 827–9.
- [2] Deegan R. D., Bakajin O., Dupont T. F., Huber G., Nagel S. R. and Witten T. A., 2000, Contact line deposits in an evaporating drop, *Phys. Rev. E* 62 756.
- [3] Deegan R. D., 2000, Pattern formation in drying drops, *Phys. Rev. E* 61 475–85.
- [4] Onoda G. and Somasundaran P., 1987, Two- and one-dimensional flocculation of silica spheres on substrates, *J. Colloid Interface Sci.* 118 169–75.
- [5] Maenosono S., Dushkin C. D., Saita S. and Yamaguchi Y., 1999, Growth of a semiconductor nanoparticle ring during the drying of a suspension droplet, *Langmuir* 15 957–65.
- [6] Shmuylovich L., Shen A. Q. and Stone H. A., 2002, Surface morphology of drying latex films: multiple ring formation, *Langmuir* 18 3441–5.
- [7] Hu H. and Larson R. G., 2006, Marangoni effect reversed coffee-ring depositions, *J. Phys. Chem. B* 110 7090–4.
- [8] Bhardwaj R., Fang X. and Attinger D., 2009, Pattern formation during the evaporation of a colloidal nanoliter drop: a numerical and experimental study, *New Journal of Physics* 11 075020.
- [9] Fischer B. J., 2002, Particle convection in an evaporating droplet, *Langmuir* 18 60–7.
- [13] Grandas, L., Reynard, C., Santini, R., Tadrist, L., (2005), Experimental study of the evaporation of a sessile drop on a heated wall. Wetting influence, *Int. J. of Thermal Sciences* 44, 137-146.
- [14] Ait saada, M., Chikh, S., & Tadrist, L., (2013), Evaporation of a sessile drop with pinned or receding contact line on a substrate with different thermophysical properties. *International Journal of Heat and Mass Transfer*, 58 (1), 197-208.
- [15] Bouchenna, C., Ait saada, M., Chikh, S., & Tadrist, L. (2015), Investigation of Thermo-Capillary Flow Inside an Evaporating Pinned Water Droplet. *Interfacial Phenomena and Heat Transfer*, 3 (2).
- [16] Raznjevic, K., Handbook of Thermodynamic Tables, Begell House, New York, (1995).
- [17] Patankar, S. V. and Spalding, D.B. (1972), A calculation procedure for heat, mass and momentum transfer in three-dimensional parabolic flows, *Int. J. of Heat and Mass Transfer*, Volume 15, Issue 10, October 1972.